Discrete Dipole Approximation with Surface Interaction DDA-SI for MATLAB™ User Guide

Vincent Loke
loke@physics.uq.edu.au
Beta version

April 11, 2011

License

0.1 Standard DDA for MATLAB™

0.2 DDA-SI

Contents

List of Figures

List of Tables

Part I

Introduction

1 Development of discrete dipole approximation (DDA)

The discrete dipole approximation (DDA) method, also referred to as the coupled dipole method (CDM), was first introduced by Purcell & Pennypacker (1973) for modelling light scattering from arbitrarily-shaped, inhomogeneous and anisotropic objects, ranging from nanometers to microns in size. It was later popularized by Draine & Flatau (1994) who released DDSCAT, an open source DDA software package written in Fortran. Amongst others, another popular and notable open source package is Amsterdam DDA (ADDA), written in C by Yurkin et al. (2007), who also reviewed different implementations and approaches to DDA and their comparative performances (Yurkin & Hoekstra, 2007). Various light scattering theories, including DDA, were compared and discussed by Kahnert et al. (2003); Wriedt (2009).

The standard DDA implementation was designed for the interaction of EM waves with objects in free space. To model light scattering from particles on a planar surface, Taubenblatt & Tran (1993) added the surface interaction capability in their Fortran implementation of DDA. Later Schmehl et al. (1997); Nebeker (1998) implemented DDSURF, also written in Fortran, and released the compiled executable. Neither of the surface-enabled DDA source codes were made available to the general public. This paper accompanies the release a set of MATLAB toolboxes, comprising DDA with surface interaction (Loke & Mengüç, 2010) called DDA-SI, the standard free-space DDA and other tools for light scattering calculations.

The initial implementation of DDA-SI is limited to light scattering from particles on a homogeneous substrate. In academic and industrial laboratories, planar substrates are often stratified, i.e., they may have one of more layers of film. The filmed surface implementation, called DDFILM, was developed by Zhang & Hirleman (2002). Later a variation called DDEFILM was developed by Bae et al. (2008) for particles embedded in the film. Another variation is DDSUB by Nebeker (1998), for subsurface particles. However, none of the abovementioned software nor source are publicly available. We prioritize further development of DDA-SI towards stratified substrate capability. This requires additional terms in the Green's tensor to account reflections off the other surfaces.

DDA is mostly limited to non-magnetic scatterers given that most scatterers produce very little magnetic effects, especially in the visible light regime. Nonetheless, various versions of magnetically-capable DDA or equivalent have been implemented by Mulholland et al. (1994); Lemaire (1997); Chaumet &

Rahmani (2009). The inclusion of magnetic dipoles into DDA will see wider applications in astrophysics, magnetic nanoantennae and other systems containing magnetic scatterers. This feature will be incorporated into later releases.

2 Software

The DDA and DDA-SI toolboxes can be downloaded from Scattport (`www.scattport.org/index.php/programs-menu/DDA-SI-menu`). This includes the current and past versions as well as the user manual which contains details on usage of the functions in the toolbox.

The toolboxes and manual can be downloaded from `www.scattport.org/index.php/programs-menu/DDA-SI-menu`. Example implementations for different types of scattering systems and calculations are also included in the toolbox. Functions for arbitrary beam illumination, beam power, force, torque, vector spherical harmonics and other calculations are packaged in the *Optical Tweezers Computational Toolbox* (`www.physics.uq.edu.au/people/nieminen/software.html`) developed by Nieminen et al. (2007).

The main disadvantage of MATLAB, an interpreted language, is its speed of execution of loops in comparison to compiled code written in languages such as C or Fortran. However, we have offset this to a certain extent by providing an option to use a wrapper function that calls a pre-compiled function written in C to perform the Sommerfeld integration. This is achieved via a MEX file (`www.mathworks.com/help/techdoc/ref/mex.html`) built under the MATLAB command line utilizing the external GNU C (gcc) compiler. In subsequent releases, the MEX wrapper can be extended to the time-consuming double-loop routine which assembles the interaction matrix. Loops aside, the matrix and vector manipulation functions in MATLAB, particularly the iterative solvers, are fast; this is due the the fact that they are written in C.

There are a number of reasons why we persist with MATLAB. The main reason is that we exploit MATLAB's fourth generation language ease of implementation and hence speed development, especially for prototype concepts. Its capability in displaying data in a multitude of ways aids development, debugging and presentation for a quick intuitive feel of the results. There is also the popularity of MATLAB as a scientific, mathematical and engineering computational language amongst lecturers, researchers and students. These are also the reasons why we implemented the *Optical Tweezers Computational Toolbox* (Nieminen et al., 2007) in MATLAB, which, together with the DDA and DDA-SI toolboxes are part of an ongoing development of a suite of tools for modelling light interaction with matter.

3 User guide

This document relates the theory to the functions that are available in the DDA and DDA-SI toolboxes

Assumes familiarity with MATLAB and EM theory

Part II

Standard DDA

4 Discrete dipole approximation (DDA) theory

TODO

- Rayleigh scatterers
- cubic lattice,
- random molecular, polarizability refractive index lattice spacing dependent

In addition to the incident field $\mathbf{E}_{inc,j}$ an each dipole, there are the field contributions from other re-radiating dipoles. The radiation from the other dipoles are assumed to be instantaneous given such short distances. Let $\mathbf{E}_j$ be the time harmonic E-field amplitude at each dipole location $\mathbf{r}_j$ due to the incident field $\mathbf{E}_{inc,j} = \mathbf{E}_0 exp(\mathrm{i}kr_j - \mathrm{i}\omega t)$ plus contributions from $N-1$ dipoles. A system of equations can be initially constructed as follows:

$$\mathbf{E}_j = \mathbf{E}_{inc,j} - \sum_{k \neq j} \mathbf{A}_{jk}\mathbf{P}_k, \tag{1}$$

where $\mathbf{A}_{jk}$ is the tensor that represents the interaction between a receiving dipole at $\mathbf{r}_j$ and the radiating dipole at $\mathbf{r}_k$. The off-diagonal block 3×3 tensor in the interaction matrix is

$$\mathbf{A}_{jk} = \frac{exp(\mathrm{i}kr_{jk})}{r_{jk}} \times \left[k^2(\hat{r}_{jk}\hat{r}_{jk} - \mathbf{1}_3) + \frac{\mathrm{i}kr_{jk} - 1}{r_{jk}^2}(3\hat{r}_{jk}\hat{r}_{jk} - I_3) \right], \quad j \neq k, \tag{2}$$

where r_{jk} is the distance from points r_j to r_k, $\hat{r}_{jk}$ is the unit vector in the direction from points r_j to r_k. The dipole interaction tensor is related to the Green's tensor $\mathbf{G}_{jk}$ of the electric field from the radiating dipole, i.e., $\mathbf{A}_{jk} = k^2\mathbf{G}_{jk}$. The derivation of the Green's tensor from the vector Helmholtz equation is shown in Jackson (1998). From (8) we can define the diagonal tensors as $\mathbf{A}_{jj} = \alpha_j^{-1}$, and substituting into (1) gives

$$\mathbf{E}_{inc,j} = \mathbf{A}_{jj}\mathbf{P}_j + \sum_{k \neq j} \mathbf{A}_{jk}\mathbf{P}_k. \tag{3}$$

The above equation can be simplified by combining the two matrices since their non-zeros tensors do not overlap. We are left with solving $3N$ unknown dipole moments $\mathbf{P}_j$ in the following exactly determined system of $3N$ linear equations (Fig. 1):

$$\sum_{k=1}^{N} \mathbf{A}_{jk}\mathbf{P}_j = \mathbf{E}_{inc,j}. \tag{4}$$

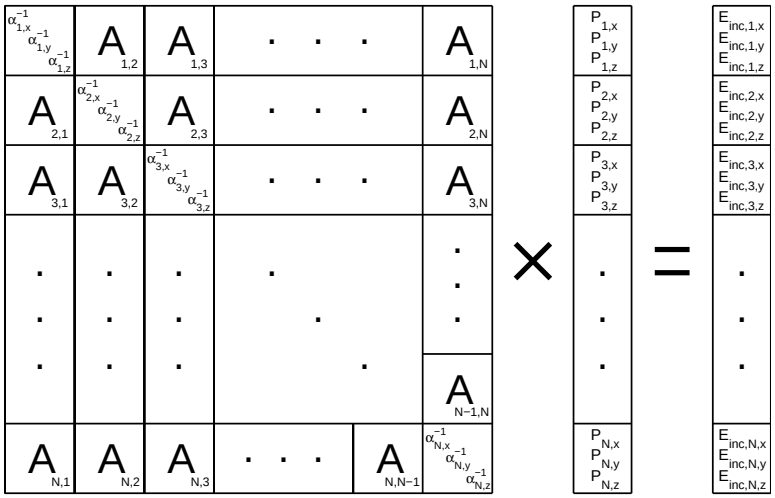

Figure 1: The system of equations comprises the interaction matrix ($\mathbf{A}$), the unknown dipole moments ($\mathbf{P}$) and the incident field ($\mathbf{E_{inc}}$). $\mathbf{A}$ is a square matrix containing $N \times N$ of $\mathbf{A}_{jk}$ 3×3 tensors, where N is the number of dipoles.

5 DDA toolbox

5.1 Calculation steps

The primary objective of DDA is to calculate the x, y and z components of the dipole moment $\mathbf{P}_j$ of each dipole. The DDA calculation involves solving a system of linear equations (Fig. 1) where $\mathbf{P}_j$ are the unknowns; it is usually performed in the following steps:

1. load or create the coordinates of the dipoles,
2. load or assign the polarizability α_j to each dipole,
3. calculated the incident field $\mathbf{E}_{\mathrm{inc},j}$ at each dipole,
4. assemble the interaction matrix $\mathbf{A}$ and
5. solve for $\mathbf{P}$ in the system of linear equations

Knowing $\mathbf{P}_j$, other quantities such as the scattered field, dipole force, Poynting vector, extinction, absorption and scattering cross sections, phase function, Mueller matrix etc. can be calculated.

5.2 Dipole coordinates

The scattering object is represented by point dipoles which are essentially Rayleigh scatterers, numbered $j = 1, ..., N$ with polarizabilities α_j located at positions $\mathbf{r}_j$. The shape file containing the dipole coordinates is usually read from a text file in using `r=dlmread('mycoordinates.txt')`. The text file format for N number of dipoles is as follows:

$$\begin{array}{ccc} x_1, & y_1, & z_1 \\ x_2, & y_2, & z_2 \\ . & . & . \\ . & . & . \\ . & . & . \\ x_N, & y_N, & z_N \end{array}$$

The variable `r` is an $N \times 3$ array (matrix). The values for the coordinates should be converted to wavelength units if they are not already so.

The standard DDA uses the Cartesian coordinate system and the dipoles are packed in a cubic lattice. The number of dipoles required to represent the scatterer and the minimal lattice spacing is determined by Draine & Flatau (1994) using the volume relation:

$$Nd^3 = \frac{4}{3}\pi a^3, \tag{5}$$

where the LHS is the cubic volume of the space occupied by the N-dipole lattice with spacing d and the RHS is the volume of the equivalent sphere with radius a. Thus, the effective radius,

$$a = d\left(\frac{3N}{4\pi}\right)^{\frac{1}{3}}. \tag{6}$$

The lattice spacing, relative to the wavelength of the incident light, has to be sufficiently small such that

$$d \leq \frac{1}{k|m|}. \tag{7}$$

For glass in air, it is required that $d < 0.12$. On the hand, lattice spacings in the order of $d < 0.01$ are required for noble metals due to their high imaginary component of their refractive indices especially at shorter wavelengths.

5.3 Polarizability

The field $\mathbf{E}_j$ at a particular dipole causes it to be polarized or acquire a dipole moment $\mathbf{P}_j$. The extent to which this occurs is determined by a quantity called

polarizability α_j. The dipole moment is thus

$$\mathbf{P}_j = \alpha_j \mathbf{E}_j, \tag{8}$$

where α_j is the polarizability tensor at each dipole (Draine & Flatau, 1994).

The original implementation of DDA Purcell & Pennypacker (1973) used the Clausius-Mossotti polarizability, given by

$$\alpha_j^{CM} = \frac{3d^3}{4\pi}(\frac{m_j^2-1}{m_j^2+2}) = \frac{3d^3}{4\pi}(\frac{\epsilon_j-1}{\epsilon_j+2}). \tag{9}$$

Subsequent corrections by Goedecke & O'Brien (1988); Hage & Greenberg (1990); Dungey & Bohren (1991) have been made to this calculation. The current most popular form, the lattice dispersion relation (LDR), was derived by Draine & Goodman (1993):

$$\alpha_j^{LDR} = \frac{\alpha_j^{CM}}{1+\frac{\alpha_j^{CM}}{d^3}[(b_1+m^2b_2+m^2b_3S)(kd)^2-\frac{2}{3}\mathrm{i}(kd)^3]}, \tag{10}$$

$$b_1 = -1.891531, b_2 = 0.1648469,$$

$$b_3 = -1.7700004, S \equiv \sum_{j=1}^{3}(\hat{a}_j\hat{e}_j)^2,$$

where $\hat{a}$ and $\hat{e}$ are unit vectors defining the direction and polarization of the incident light.

The polarizability of each dipole can be different in the x, y and z directions for anisotropic substances and different from the other dipoles for inhomogeneous materials. The polarizability values are arranged in the same sequence as the dipole coordinates. However, they are transposed from $N \times 3$ to the $3N \times 1$ array of $\alpha_{x_1}, \alpha_{y_1}, \alpha_{z_1}, \alpha_{x_2}, \alpha_{y_2}, \alpha_{z_2}, ..., \alpha_{x_N}, \alpha_{y_N}, \alpha_{z_N}$, so that the inverse polarizabilities can conveniently fit into the diagonal of the interaction matrix when compacting (3) into (4).

The polarizability values can be loaded from a text file, as with the coordinates, in the $N \times 3$ format, then transposed to $3N \times 1$:

```
alph = dlmread('mypolarizabilities.txt');
alph = col3to1(alph); (utility function included in the toolbox)
```

In many cases, we only know the relative refractive index (or indices) but not the polarizabilities, in which case, they can be calculated using

```
function alph = polarizability_LDR(d,m,kvec,E0)
k = 2*pi;
```

```
N = length(m); % number of dipoles
b1 = -1.8915316;
b2 = 0.1648469;
b3 = -1.7700004;
a_hat = kvec/norm(kvec);
e_hat = E0/norm(E0);
S = 0;

for j = 1:3
 S = S + (a_hat(j)*e_hat(j))^2;
end

alpha_CM = 3*d^3/(4*pi)*(m.^2 - 1)./(m.^2 + 2); % Clausius-Mossotti
alpha_LDR = alpha_CM./...
 (1 + (alpha_CM/d^3).*((b1+m.^2*b2+m.^2*b3*S)*(k*d)^2-2/3*i*k^3*d^3));
alph = col3to1([alpha_LDR'; alpha_LDR'; alpha_LDR'])
```

In the initial release of the toolbox, the above function caters for isotropic substances only, i.e., the polarizability of a dipole the same in x, y and z-directions. However, the anisotropic feature can be easily implemented; the function (10) can be calculated for each axis. Form birefringence, on the other hand, can be achieved via the arrangement of the dipoles.

The scatterer can be homogeneous or made from composite materials. It is a matter of having different sets of polarizabilities, calculated for corresponding dipoles coordinates, for different materials. For example, if a silica sphere is coated with a layer of gold, there will be 2 sets of appended coordinates and their corresponding polarizabilities.

5.4 The incident E-field

The scatterer(s) may be illuminated by any form incident electric field, the simplest being the plane wave. For the calculation of the E-field of each dipole at r_j, we leave out time harmonic component iωt of the E-field and just use $\mathbf{E}_{inc,j} = \mathbf{E}_0 exp(\mathrm{i}\mathbf{k}r_j)$ in the function:

```
function Ei = E_inc(E0,kvec,r)
[N,cols] = size(r);
D = ones(N,1);
kr = dot([kvec(1)*D kvec(2)*D kvec(3)*D],r,2);
expikr = exp(i*kr);
E1 = [E0(1)*expikr E0(2)*expikr E0(3)*expikr];
Ei = col3to1(E1);
```

For example, the wave vector $\mathbf{k} = (0, 0, 1)$ and the unit vector $\hat{e}_0 = (1, 0, 0)$ means that the plane wave propagates in the z-direction and is x-polarized. If the plane wave has left-circular polarization and propagates in y-direction, $\mathbf{k} = (0, 1, 0)$ and $\hat{e}_0 = (1, 0, i)$. For wave vectors that are not aligned with any axis, the unit vector of the incident field $\hat{e}_0$ and the wave vector $\mathbf{k}$ given an

arbitrary incident angle is calculated using simple trigonometry.

Arbitrary incident light, e.g., a tightly-focused Gaussian laser beam, a Laguerre-Gauss donut beam, a Bessel beam, or even a plane wave can be modelled using beam shape coefficients (Nieminen et al., 2003b). These coefficients represent the amplitudes of the modes of the vector spherical wave functions (Mischenko et al., 2000) which form exact representations of the ideal beam. Details for calculating the incident field at the dipoles illuminated by and arbitrary beam are explained in the toolbox user manual.

5.5 Constructing the interaction matrix

The interaction matrix is constructed by looping from dipoles $j = 1...N$. The 'self-interaction' of a dipole is just the reciprocal of its polarizability as shown in the block diagonal in figure 1. The block off-diagonals are the Green's tensors for the receiving dipoles at r_j and the radiating dipoles at r_k, $k = 1...N$, are defined as follows:

$$\mathbf{A}_{jk} = -\frac{k_0^2 \exp(\mathrm{i}k_0 r_{jk})}{r_{jk}} \begin{bmatrix} \beta_{jk} + \gamma_{jk}\hat{r}_{jk,x}^2 & \gamma_{jk}\hat{r}_{jk,x}\hat{r}_{jk,y} & \gamma_{jk}\hat{r}_{jk,x}\hat{r}_{jk,z} \\ \gamma_{jk}\hat{r}_{jk,y}\hat{r}_{jk,x} & \beta_{jk} + \gamma_{jk}\hat{r}_{jk,y}^2 & \gamma_{jk}\hat{r}_{jk,y}\hat{r}_{jk,z} \\ \gamma_{jk}\hat{r}_{jk,z}\hat{r}_{jk,x} & \gamma_{jk}\hat{r}_{jk,z}\hat{r}_{jk,y} & \beta_{jk} + \gamma_{jk}\hat{r}_{jk,z}^2 \end{bmatrix} \tag{11}$$

where

$$r_{jk} = [(x_j - x_k)^2 + (y_j - y_k)^2 + (z_j - z_k)^2]^{1/2}, \tag{12}$$

$$\hat{r}_{jk,x} = \frac{r_{jk,x}}{r_{jk}}, \quad \hat{r}_{jk,y} = \frac{r_{jk,y}}{r_{jk}}, \quad \hat{r}_{jk,z} = \frac{r_{jk,z}}{r_{jk}}, \tag{13}$$

$$\beta_{jk} = [\mathbf{1} - (k_0 r_{jk})^{-2} + \mathrm{i}(k_0 r_{jk})^{-1}], \tag{14}$$

$$\gamma_{jk} = -[\mathbf{1} - 3(k_0 r_{jk})^{-2} + 3\mathrm{i}(k_0 r_{jk})^{-1}]; \tag{15}$$

The function for calculating the interaction matrix is

```
function A = interaction_A(k,r,alph)
[N,dummy] = size(r);
A = single(zeros(3*N,3*N));
I = eye(3);

for jj=1:N
 for kk=1:N
  if jj  = kk
   rk_to_rj = r(jj,:)-r(kk,:);
   rjk = norm(rk_to_rj);
   rjk_hat = (rk_to_rj)/rjk;
   rjkrjk = rjk_hat'*rjk_hat;
```

```
    Ajk = exp(i*k*rjk)/rjk*...
          ((k^2*(rjkrjk - I) + i*k*rjk-1)/rjk^2*(3*rjkrjk - I));
    A((jj-1)*3+1:jj*3,(kk-1)*3+1:kk*3) = Ajk;
   else
    A((jj-1)*3+1,(kk-1)*3+1) = 1/alph((jj-1)*3+1);
    A((jj-1)*3+2,(kk-1)*3+2) = 1/alph((jj-1)*3+2);
    A((jj-1)*3+3,(kk-1)*3+3) = 1/alph((jj-1)*3+3);
   end
  end
end
```

Alternatively, the variable `A` can be declared global which saves memory by only keeping one copy the variable. To do this, delclare '`global A`' in the main or calling script and use `interaction_A_glob(k, r, alph)` instead.

The interaction matrix, which has complex elements, is the component that takes up most of the RAM during the calculation; its memory requirements scales with $(3N)^2$. The single and double precision interaction matrices consume $8 \times (3N)^2$ bytes and $16 \times (3N)^2$ bytes respectively.

5.6 Solving the system of equations

We have a system of linear equations (Fig. 1), $\mathbf{AP} = \mathbf{E}_{inc}$. Due to the size of linear system for most DDA calculations, the MATLAB backslash operator `P = A\Ei` is not the method of choice for solving `P`. The problem lies not with its accuracy when computing the least squares solution, rather, it is very slow compared with other sufficiently accurate methods. The recommended functions are the iterative methods `minres(A,Ei)`, `gmres(A,Ei)` or `qmr(A,Ei)`.

5.7 Extinction, scattering and absorption cross-sections

The extinction and absorption cross sections can be calculated, as defined in Draine (1988):

$$C_{\text{ext}} = \frac{4\pi k}{|\mathbf{E}_0|^2} \sum_{j=1}^{N} \text{Im}\left(\mathbf{E}^*_{\text{inc},j} \cdot \mathbf{P}_j\right), \tag{16}$$

$$C_{\text{abs}} = \frac{4\pi k}{|\mathbf{E}_0|^2} \sum_{j=1}^{N} \left\{ \text{Im}\left[\mathbf{P}_j \cdot (\alpha_j^{-1})^* \mathbf{P}_j^*\right] - \frac{2}{3} k^3 |\mathbf{P}_j|^2 \right\}, \tag{17}$$

and the scattering cross section $C_{\text{sca}} = C_{\text{ext}} - C_{\text{abs}}$. The absorption and extinction cross section functions are:

```
function C = C_abs(k, E0, P, alph)
C = 4*pi*k/norm(E0)^2*(-imag(dot(P,P./alph)) - 2/3*k^3*dot(P,P));
```

and

```
function C = C_ext(k, E0, Ei, P)
C = 4*pi*k/sum(abs(E0.^2))*imag(dot(Ei,P));
```

respectively. These quantities are often expressed in terms of extinction, absorption and scattering efficiencies, i.e., the cross section divided by the cross-sectional area of the scatterer. In the case of a sphere, the extinction efficiency is defined as $Q_{\mathrm{ext}} = C_{\mathrm{ext}}/(\pi a^2)$, where a is the radius of the sphere. Similarly, the absorption and scattering efficiencies are defined, respectively, as $Q_{\mathrm{abs}} = C_{\mathrm{abs}}/(\pi a^2)$ and $Q_{\mathrm{sca}} = C_{\mathrm{sca}}/(\pi a^2)$.

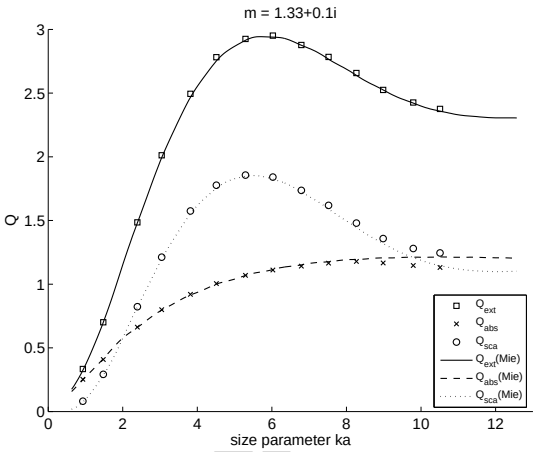

Figure 2: The extinction, absorption and scattering efficiencies of fictitious absorbing water spheres ($n = 1.33 + 0.1i$) versus the size parameter. DDA is benchmarked against the Mie theory.

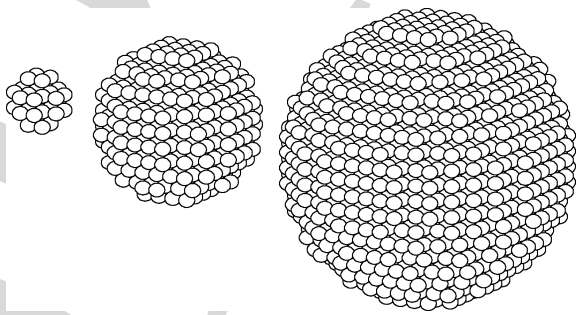

Figure 3: Pseudospheres made from 32, 552 and 3112 dipoles, arranged in cubic lattices.

Figure 2 shows the extinction efficiency of a spheres, with refractive index $n = 1.33 + 0.1i$, as a function of the diameter calculated via a DDA and the Mie theory. The DDA pseudo sphere is scaled to achieve the correct diameter whist observing the minimum required number of dipoles (5) and the maximum

allowable lattice spacing (7). The following listing demonstrates the calculation of extinction, absorption and scattering cross-sections and efficiencies:

```
E0 = [1 1 0];
m1 = 1.33 + .1i;
k = 2*pi;
d = 1/(abs(m1)*k);
nrange = [8 32 136 280 552 912 1472 2176 3112 4224 5616 7208 9328 11536];
arange = (3*nrange/(4*pi)).^(1/3) * d;

Csca = zeros(1,length(nrange));
Cabs = zeros(1,length(nrange));
Cext = zeros(1,length(nrange));

ix = 0;
for N = nrange % number of dipoles
  ix = ix+1;
  m = m1*ones(N,1);
  kvec = [0 0 k];
  rfile = ['sphere_' int2str(nrange(ix)) '.txt'];
  S=dlmread(rfile);
  r = d*[S(:,1) S(:,2) S(:,3)];
  Ei = E_inc(E0, kvec, r);
  alph = polarizability(d,m,k);
  A = interaction_A(k, r, alph);
  P = gmres(A,Ei);

  Cext(ix) = C_ext(k,E0,Ei,P);
  Cabs(ix) = C_abs(k,E0,Ei,P,alph);
  Csca(ix) = Cext(ix) - Cabs(ix);
end

ix = 0;
range = 0.1:0.01:2;
Qext_Mie = zeros(1,length(range));
Qabs_Mie = zeros(1,length(range));
Qsca_Mie = zeros(1,length(range));
for a = range;
ix = ix + 1;
ka = k*a;
res = Mie(m1,ka);
Qext_Mie(ix) = res(1);
Qabs_Mie(ix) = res(3);
Qsca_Mie(ix) = res(2);
end
```

5.8 The scattered and total E-field

The scattered **E**-field at any point **r** (relative to the origin) can be calculated by adding up the contributions from each dipole using the electric dipole field equation from section 9.2 of Jackson (1998),

$$\mathbf{E}_{sca}(k\mathbf{r}) = \frac{1}{4\pi\epsilon_0}\left\{k^2(\hat{\mathbf{r}}\times\mathbf{p})\times\hat{\mathbf{r}}\frac{e^{\mathrm{i}kr}}{r} + [3\hat{\mathbf{r}}(\hat{\mathbf{r}}\cdot\mathbf{p}) - \mathbf{p}]\left(\frac{1}{r^3} - \frac{\mathrm{i}k}{r^2}\right)e^{\mathrm{i}kr}\right\}, \quad (18)$$

The toolbox function for calculating the E-field at evaluation point `r_E` is

```
function E = E_sca(k0,r,P,r_E)
[N,dummy] = size(r);
E = zeros(1,3);
I = eye(3);


for j = 1:N
  rEj = r_E-r(j,:); % dipole to evaluation point vector
  r_mag = norm(rEj); % magnitude of the vector
  rEj_hat = rEj/r_mag;
  rEjrEj = rEj_hat'*rEj_hat;
  E = E + (exp(i*k0*r_mag)/r_mag*...
           (k0^2*(rEjrEj - I) + (i*k0*r_mag-1)/r_mag^2*(3*rEjrEj - I))*...
                                  P(3*(j-1)+1:3*(j-1)+3))';
end
```

In the far field zone, defined as at any given point that is much farther than the intra-dipole distances ($\mathbf{r} >> \mathbf{r}_j$), the $1/r^2$ and $1/r^3$ terms in (18) can be ignored as their contributions diminish rapidly with distance; the scattered field approaches:

$$\mathbf{E}^{\mathrm{FF}}_{sca}(k\mathbf{r}) = \frac{1}{4\pi\epsilon_0}\left\{k^2(\hat{\mathbf{r}}\times\mathbf{p})\times\hat{\mathbf{r}}\frac{e^{\mathrm{i}kr}}{r}\right\}. \quad (19)$$

The corresponding toolbox function usage is

```
function E = E_sca_FF(k,r,P,r_E)
[N,cols] = size(r);
E = 0;
r_norm = norm(r_E);
r_hat = r_E/r_norm;


for j = 1:N
  E = E + exp(-i*k*dot(r_hat,r(j,:)))*(r_hat'*r_hat - eye(3))*P(3*(j-1)+1:3*(j-1)+3);
end
E = E*k^2*exp(i*k*r_norm)/r_norm;
```

where `r` can be a single point (x, y, z) or an $N \times 3$ array of points but `r_E` is an single evaluation point. After calculating the scattered field, the total field can

be determined by the superposition of the incident and scattered fields,

$$\mathbf{E}_{tot}(k\mathbf{r}) = \mathbf{E}_{inc}(k\mathbf{r}) + \mathbf{E}_{sca}(k\mathbf{r}); \tag{20}$$

To calculate the field intensities at the array of points, we simply use the dot product function, i.e., `I=dot(E,E,2)`.

5.9 Phase function

The scattering phase function is a means of characterizing one of the main scattering properties of a particle (van de Hulst, 1957); it is the scattered intensity in the far field versus the scattering angle, normalized against the intensity at the angle (0°),

$$\Phi(\theta) = \frac{I(\theta)}{I(0^\circ)} \tag{21}$$

Figure 4 shows the scattering geometry for the phase function, which is usually calculated or measure in two planes, one parallel and the other perpendicular to the plane of polarization of the incident plane wave.

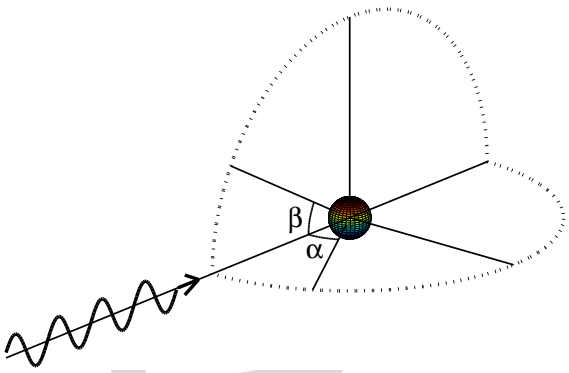

Figure 4: The schematic for angles at which the scattered intensity are measured or calculated; β sweeps along the plane of the polarization of the incident plane wave and α along the perpendicular.

```
E0 = [1 0 0]; % x-polarization
m1 = 1.33;
rfile = ['sphere_552.txt'];
S = dlmread(rfile);
N = length(S(:,1))


k = 2*pi; % wave number
d = 1/(abs(m1)*k);
a_eff = (3*N/(4*pi))^(1/3)*1/(k*abs(m1));
r = d*[S(:,1) S(:,2) S(:,3)];
m = m1*ones(N,1);
```

```
kvec = [0 0 k]; % propagating in +z direction
Ei = E_inc(E0,kvec,r);
alph = polarizability(d,m,k);
A = interaction_A(k,r,alph);
P = gmres(A,Ei);


th = linspace(0,pi,100);
Esca_S = zeros(1,length(th));
Esca_P = zeros(1,length(th));
Einc_S = zeros(1,length(th));
Einc_P = zeros(1,length(th));


ix = 0;
for theta = th
  ix = ix+1;


  phi = 90; % perpendicular to x-z plane
  r_E = zeros(1,3); % evaluation point
  [r_E(1) r_E(2) r_E(3)] = rtp2xyz(100, theta, phi);
  E = E_sca_FF(k,r,P,r_E);
  Esca_S(ix) = norm(E);
  kr = dot([k k k],r_E,2);
  expikr = exp(i.*kr);
  E1 = [E0(1)*expikr E0(2)*expikr E0(3)*expikr];
  Einc_S(ix) = norm(E1);


  phi = 0; % parallel to x-z plane
  r_E = zeros(1,3);
  [r_E(1) r_E(2) r_E(3)] = rtp2xyz(100, theta, phi);
  E = E_sca_FF(k,r,P,r_E);
  Esca_P(ix) = norm(E);
  kr = dot([k k k],r_E,2);
  expikr = exp(i.*kr);
  E1 = [E0(1)*expikr E0(2)*expikr E0(3)*expikr];
  Einc_P(ix) = norm(E1);
end


semilogy(th*180/pi,Esca_P.^2./Einc_P.^2,'--',th*180/pi,Esca_S.^2./Einc_S.^2)
```

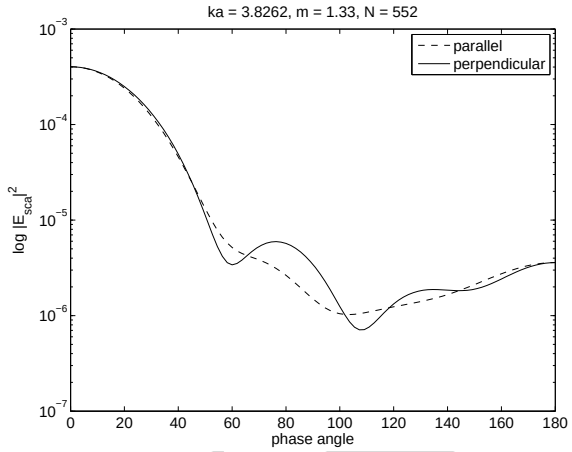

Figure 5:

Part III

DDA for symmetrical objects

5.10 Formulating the T-matrix via DDA and exploiting rotational symmetry

The extended boundary condition method (EBCM) or null-field method (NFM) developed by Waterman (1971) was first used to formulate the T-matrix; EBCM is often synonymously referred to as the *T-matrix method*. However, any valid method for calculating light interaction with matter can be used to calculate the T-matrix. DDA is such a method as demonstrated by Mackowski (2002) and Loke et al. (2009). We include the function for calculating the T-matrix via the near-field point matching (Loke et al., 2009) scheme in the first release and the far-field point matching Loke et al. (2010) will follow in subsequent releases.

The fields of the incident ($\mathbf{E}_{inc}$) and scattered ($\mathbf{E}_{sca}$) light for an illuminated particle in free space can be represented in terms of vector spherical wave functions (VSWFs)(Waterman, 1971; Mishchenko, 1991; Nieminen et al., 2003b,a):

$$\mathbf{E}_{\text{inc}} = \sum_{n=1}^{\infty} \sum_{m=-n}^{n} a_{nm}\mathbf{M}_{nm}^{(3)}(kr) + b_{nm}\mathbf{N}_{nm}^{(3)}(kr), \tag{22}$$

$$\mathbf{E}_{\text{sca}} = \sum_{n=1}^{\infty} \sum_{m=-n}^{n} p_{nm}\mathbf{M}_{nm}^{(1)}(kr) + q_{nm}\mathbf{N}_{nm}^{(1)}(kr). \tag{23}$$

where $\mathbf{M}_{nm}^{(3)}$ & $\mathbf{N}_{nm}^{(3)}$ are regular VSWFs, $\mathbf{M}_{nm}^{(1)}$ & $\mathbf{N}_{nm}^{(1)}$ are the outward-propagating VSWFs, n & m are radial and azimuthal modes respectively and the incident and scattered coefficients are connected by the T-matrix (Waterman, 1971;

Mishchenko, 1991):

$$\begin{bmatrix} p_{nm} \\ q_{nm} \end{bmatrix} = \mathbf{T} \begin{bmatrix} a_{nm} \\ b_{nm} \end{bmatrix}. \tag{24}$$

Put another way, the light scattering characteristics of the particle, for a given wavelength, is encapsulated in the T-matrix. The T-matrix need only be calculated once and its advantage come to the forth when repeated calculation by varying illumination is required; given a set of incident coefficients, the scattering coefficients and be calculated in a matter of seconds.

Some scatterers may be excessively large to a point where the computer RAM may be insufficient. If the scatterer possesses discrete rotational symmetry, such as a microrotor, optimization schemes (Loke et al., 2009) can be applied to reduce the required memory and computational time by orders of magnitude. The symmetry optimized T-matrix calculation is included in the toolbox. It's extensive implementation details are covered in Loke et al..

Examples of the phase functions of cubes, using pre-calculated T-matrices, are shown in figure 6. The calculations are based on equivalent cubes of those used by Wriedt & Comberg (1998).

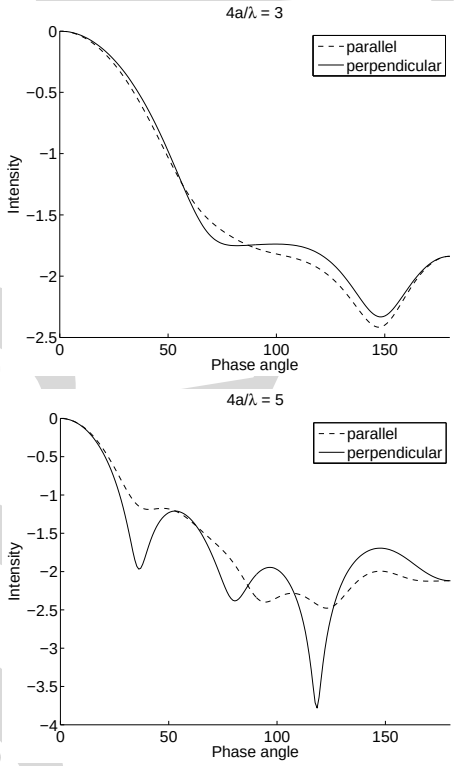

Figure 6: The phase function for cubes with the refractive index of 1.5 and widths of a) 0.75λ b) 1.25λ.

Part IV

DDA with surface interaction (DDA-SI)

DDA was designed for free-space light scattering and does not account for surface interactions when the scatterer is near a surface. In the presence of a surface, we have to consider three aspects. Firstly, if the illumination originates from the same medium where the scatterer resides, the incident field results from the superposition of the direct and reflected incident light (Fig. 7). Secondly, in addition to the direct dipole-dipole interactions in standard DDA we will have to include the surface-reflected interactions (Fig. 9). Finally, when calculating the scattered field, the reflected component (Fig 12) needs to be included. The DDA-SI toolbox is a MATLAB implementation of DDA with surface interaction (Loke & Mengüç, 2010).

6 The incident field

Consider that the source of illumination is a plane wave that originates from the same side of the planar interface as the scatterer, with the incident angle γ (Fig. 7). The incident electric field at the dipoles due to direct TE-polarized plane wave illumination is calculated as follows:

```
E0 = [0 1 0];
kvec = k*[sin(gamma) 0 -cos(gamma)];
Ei = E_inc(E0, kvec, r);
```

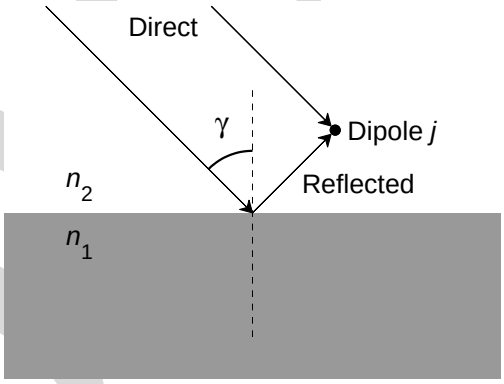

Figure 7: A dipole illuminated by the direct incident plane wave incident at angle γ and the reflected plane wave.

Figure 11b shows the axes and angle conventions used in the toolbox. The

reflected plane wave is still TE-polarized but undergoes attenuation (Fresnel reflection coefficient) and reversal in the z-direction:

```
[refl_TE,refl_TM] = Fresnel_coeff_n(n1,abs(gamma));
E0_r = refl_TE*[0 1 0];
kvec_r = k*[sin(gamma) 0 cos(gamma)];
Ei_r = E_inc(E0_r, kvec_r, r);
```

The total incident field is then `Ei + Ei_r`.

In the scenario where the source is on the opposite of the planar interface, there is no reflected component. The case of the incident plane undergoing total internal reflection is of particular interest because an evanescent field will exist along the media interface (Fig. 8); the formalism is discussed in Loke & Mengüç (2010). The following function calculates the resultant evanescent TE (`E1s`) and TM (E1p) E-field field amplitudes and complex wave vector `kvec`:

```
[kvec,E2s,E2p] = evanescent_E(E1s,E1p,gamma_2,n_1,n_2);
function [k2,E2s,E2p] = evanescent_E(E1s,E1p,theta_1,n1,n2)
```

given the incident TE (`E1s`) and TM (E1p) E-field which are alternately 1 or 0. The returned values are then passed to the standard function for calculating the E-field a the dipoles as `r`:

```
Ei = E_inc(E2s + E2p, kvec, r);
```

which returns the $N \times 3$ array of incident E-fields (`Ei`) for dipoles at `r`, due to the imaginary z-component of `kvec`, are consistent with $E_z = E_0 \exp(\mathrm{i}k_z z)$. In other words, the E-field exponentially decays in the z-direction.

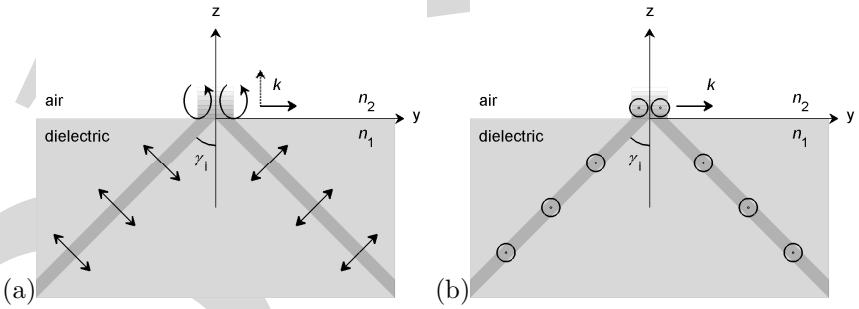

Figure 8: Total internal reflection of incident (a) TM (b) TE plane waves from below the substrate surface. Evanescent waves exists above the surface.

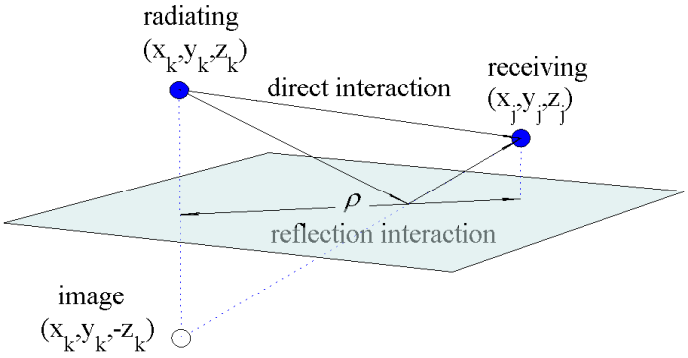

Figure 9: Radiating dipole over a surface, its image and the receiving dipole. On the surface, $z = 0$.

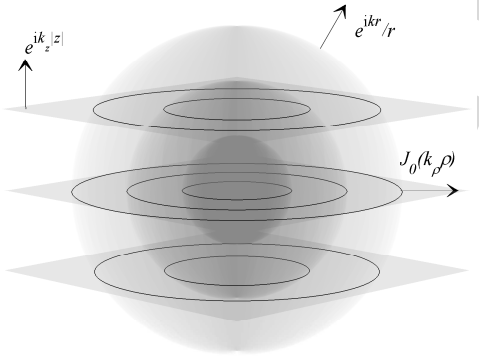

Figure 10: The spherical wave decomposed into cylindrical and planar components.

7 The interaction matrix

In the presence of at surface the Green's tensor for a dipole-dipole interaction will have two components; the system of linear equations for DDA-SI is

$$\sum_{k=1}^{N} \mathbf{A}_{jk}^{\mathrm{SI}} \mathbf{P}_k = \sum_{k=1}^{N} \left(\mathbf{A}_{jk} + \mathbf{R}_{jk} \right) \mathbf{P}_k = \mathbf{E}_{inc,j}, \tag{25}$$

where the $\mathbf{A}_{jk}$ term represents the direct interaction and is identical that in free-space DDA (11) and $\mathbf{R}_{jk}$ is the contribution from the reflected dipole interaction (Fig. 9). The reflected component is not a straight forward calculation of image Green's function. This is because the spherical wave from each dipole is only partially reflected, and not equally in all directions. Sommerfeld (1909) proposed that a spherical wave can be decomposed into cylindrical and planar components (Fig. 10). The cylindrical wave will be unperturbed because it expands parallel to the surface. The planar wave, on the other hand, propagates in direction normal to the surface and is partially reflected. The fraction of the

reflected field strength is calculated using the Fresnel coefficients for the TE and TM incident fields (Chew, 1990).

The following Sommerfeld integral is used to evaluate the Green's function of the electric field from a reflected dipole:

$$\left(\frac{e^{\mathrm{i}kr}}{4\pi r}\right)_{TE,TM} = \frac{\mathrm{i}}{4\pi}\int_0^\infty \frac{k_\rho}{k_z} J_0(k_\rho\rho) R^{TE,TM} e^{\mathrm{i}k_{2z}(z_j+j)} dk_\rho, \tag{26}$$

where J_0, the Bessel function, represents the cylindrical wave component of the expansion whereas $e^{\mathrm{i}k_{2z}(z_j+j)}$ is the planar component. By using variable substitution (Baños, 1966; Lytle & Lager, 1974), the integral is separated in to components that are evaluated using contour and numerical integration (Schmehl et al., 1997). The complicated derivation process is shown in Loke & Mengüç (2010) and the resultant reflection tensor becomes:

$$\mathbf{R}_{jk} = -\begin{bmatrix} \hat{r}^{\mathrm{I}\,2}_{jkx} I^{\mathrm{H}}_\rho - \hat{r}^{\mathrm{I}\,2}_{jky} I^{\mathrm{H}}_\phi & \hat{r}^{\mathrm{I}\,2}_{jkx}\hat{r}^{\mathrm{I}\,2}_{jky}(I^{\mathrm{H}}_\rho + I^{\mathrm{H}}_\phi) & \hat{r}^{\mathrm{I}\,2}_{jkx} I^{\mathrm{V}}_\rho \\ \hat{r}^{\mathrm{I}\,2}_{jkx}\hat{r}^{\mathrm{I}\,2}_{jky}(I^{\mathrm{H}}_\rho + I^{\mathrm{H}}_\phi) & \hat{r}^{\mathrm{I}\,2}_{jkx} I^{\mathrm{H}}_\rho - \hat{r}^{\mathrm{I}\,2}_{jky} I^{\mathrm{H}}_\phi & \hat{r}^{\mathrm{I}\,2}_{jky} I^{\mathrm{V}}_\rho \\ -\hat{r}^{\mathrm{I}\,2}_{jkx} I^{\mathrm{V}}_\rho & -\hat{r}^{\mathrm{I}\,2}_{jky} I^{\mathrm{V}}_\rho & I^{\mathrm{V}}_z \end{bmatrix} - \tag{27}$$

$$\frac{k_1^2 - k_2^2}{k_1^2 + k_2^2}\frac{\exp(\mathrm{i}k_0 r_{I,jk})}{r_{I,jk}} \begin{bmatrix} -(\beta^{\mathrm{I}}_{jk} + \gamma^{\mathrm{I}}_{jk}\hat{r}^{\mathrm{I}\,2}_{jkx}) & -\gamma^{\mathrm{I}}_{jk}\hat{r}^{\mathrm{I}\,2}_{jkx}\hat{r}^{\mathrm{I}\,2}_{jky} & \gamma^{\mathrm{I}}_{jk}\hat{r}^{\mathrm{I}\,2}_{jkx}\hat{r}^{\mathrm{I}\,2}_{jkz} \\ -\gamma^{\mathrm{I}}_{jk}\hat{r}^{\mathrm{I}\,2}_{jky}\hat{r}^{\mathrm{I}\,2}_{jkx} & -(\beta^{\mathrm{I}}_{jk} + \gamma^{\mathrm{I}}_{jk}\hat{r}^{\mathrm{I}\,2}_{jky}) & \gamma^{\mathrm{I}}_{jk}\hat{r}^{\mathrm{I}\,2}_{jky}\hat{r}^{\mathrm{I}\,2}_{jkz} \\ -\gamma^{\mathrm{I}}_{jk}\hat{r}^{\mathrm{I}\,2}_{jkz}\hat{r}^{\mathrm{I}\,2}_{jkx} & -\gamma^{\mathrm{I}}_{jk}\hat{r}^{\mathrm{I}\,2}_{jkz}\hat{r}^{\mathrm{I}\,2}_{jky} & \beta^{\mathrm{I}}_{jk} + \gamma^{\mathrm{I}}_{jk}\hat{r}^{\mathrm{I}\,2}_{jkz} \end{bmatrix},$$

where

$$r^{\mathrm{I}}_{jk} = [(x_j - x_k)^2 + (y_j - y_k)^2 + (z_j + z_k)^2]^{1/2}, \tag{28}$$

$$\hat{r}^{\mathrm{I}}_{jkx} = \frac{r^{\mathrm{I}}_{jkx}}{r^{\mathrm{I}}_{jk}}, \qquad \hat{r}^{\mathrm{I}}_{jky} = \frac{r^{\mathrm{I}}_{jky}}{r^{\mathrm{I}}_{jk}}, \qquad \hat{r}^{\mathrm{I}}_{jkz} = \frac{r^{\mathrm{I}}_{jkz}}{r^{\mathrm{I}}_{jk}} \tag{29}$$

$$\beta^{\mathrm{I}}_{jk} = [\mathbf{1} - (k_0 r^{\mathrm{I}}_{jk})^{-2} + \mathrm{i}(k_0 r^{\mathrm{I}}_{jk})^{-1}], \tag{30}$$

$$\gamma^{\mathrm{I}}_{jk} = -[\mathbf{1} - 3(k_0 r^{\mathrm{I}}_{jk})^{-2} + 3\mathrm{i}(k_0 r^{\mathrm{I}}_{jk})^{-1}], \tag{31}$$

and I^{V}_ρ, I^{V}_z, H_ρ and I^{H}_ϕ are Sommerfeld identities (Loke & Mengüç, 2010), which are evaluated using contour integration either in MATLAB or calling the a MEX (MATLAB interface compiled in C) function, to be determined by the user using a global flag. The interaction matrix in (25) is seamlessly calculated using:

```
A = interaction_AR(k1,k2,r,alph)
```

For a given number of dipoles, the size of the interaction matrix is the same as that for conventional DDA.

8 The scattered E-field in the far-field zone

The scattered field in the upper half-space is the sum of the field contributions as a result of the dipole moments of every dipole as per conventional DDA with

those from the image (reflected) dipoles (Fig. 11a). Figure 11b shows the field detection geometry. The scattering frame, on which the calculations are based,

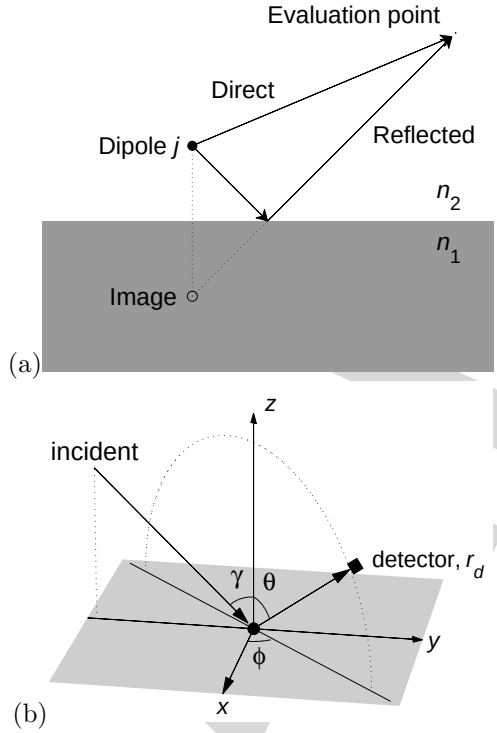

Figure 11: a) The scattered electric field. b) The scattering geometry for a particle on a surface. The direction of the incident light is defined by the angle γ from the surface normal and the incident plane coincides with $x = 0$. The scattered far field is calculated for a range of zenith angles θ along the plane at the azimuthal angle ϕ.

is shown in figure 12. In the far-field zone, the scattered E-field is calculated (Schmehl et al., 1997) using:

$$\mathbf{E}_{sca}(\mathbf{r}) = k_0^2 \frac{e^{\mathrm{i}k_0 r}}{4\pi r} \sum_{j=1}^{N} \left\{ e^{-\mathrm{i}k_{sca}.r_j} \left[(\mathbf{p}_j \cdot \hat{\mathbf{e}}_1)\hat{\mathbf{e}}_1 + (\mathbf{p}_j \cdot \hat{\mathbf{e}}_2)\hat{\mathbf{e}}_2 \right] + \right. \tag{32}$$
$$\left. e^{-\mathrm{i}k_{sca}.r_{I,j}} \left[R^{\mathrm{TM}} (\mathbf{p}_j \cdot \hat{\mathbf{e}}_1)\hat{\mathbf{e}}_1 + R^{\mathrm{TE}} (\mathbf{p}_j \cdot \hat{\mathbf{e}}_2)\hat{\mathbf{e}}_2 \right] \right\},$$

where the unit vectors $\mathbf{e}_1$ and $\mathbf{e}_2$ are the Cartesian expressions of the $\mathbf{e}_\theta$ and $\mathbf{e}_\phi$ vectors in spherical coordinates respectively, in the scattering frame (Fig. 12). The radial component of the scattered field approaches zero in the far field and thus $\mathbf{e}_r$ is irrelevant. The reflected terms in (32) are subject to the Fresnel reflection coefficients, R^{TM} and R^{TE}. The corresponding toolbox function is:

```
E = E_sca_SI(k,r,P,det_r,theta,phi,refl_TM,refl_TE)
```

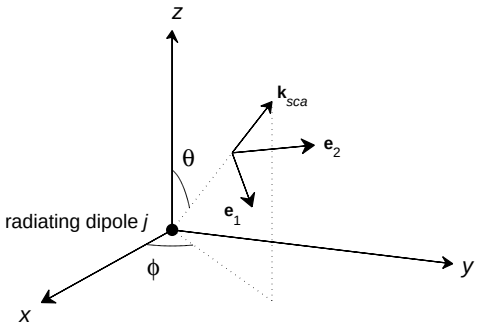

Figure 12: The scattering frame of a given dipole for calculating the scattered field.

We use the above function to calculate the scattered intensity of a particle on a Silicon substrate for a range of scattering angles (Fig. 11b) based on examples from a similar coupled dipole method by Taubenblatt & Tran (1993). Fig. 13 shows the scattered intensity of a 540 nm polystyrene sphere illuminated by an s-polarized plane wave with an incident angle of $\gamma = 0°$. The scattering profile is very sensitive to the shape, size and refractive index of the particle and can effectively be used as a 'signature to identify the particle that cannot be conventionally seen optical microscopes.

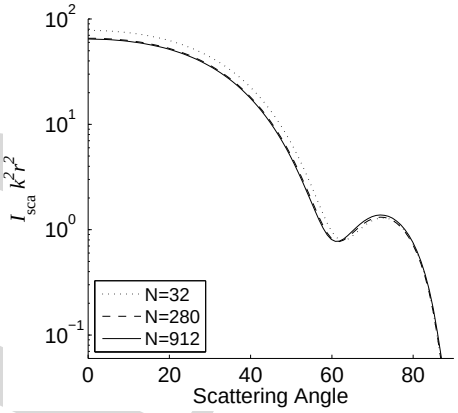

Figure 13: The scattered intensity versus the scattering angle for a 540 nm polystyrene sphere on a flat Si surface. The incident light was s-polarized, wavelength $\lambda = 632.8\ nm$ and the incident angle was $\gamma = 0°$.

In another example, Taubenblatt & Tran (1993) proposed that defects on integrated circuit structures can be detected in this manner; a 300 nm sided cube is illuminated by an s-polarized plane wave incident at $\gamma = 65°$. The scattering intensity for cubes with various defects, modelled with missing octants in the top left, top right and bottom right, are used as test cases (Fig. 14). The results from our toolbox model are similar to those of (Taubenblatt & Tran, 1993)

apart from the case of the missing top right octant.

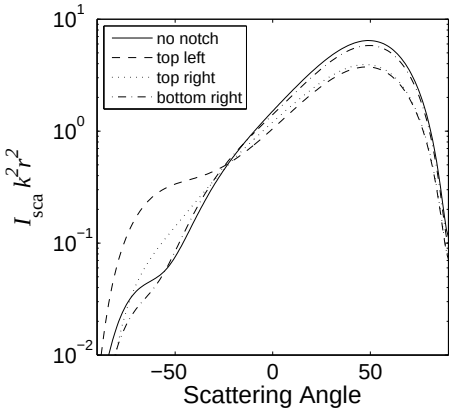

Figure 14: The scattered intensity versus the scattering angle for a 300 nm SiO cube on a flat Si surface. The incident light was p-polarized, wavelength $\lambda = 632.8\ nm$ and the incident angle was $\gamma = 65°$.

9 The internal and near-field zones

In some applications, the E-field distribution of the internal and near field is of particular interest. For example, in the study of the near-field coupling between an AFM probe on a nanoparticle on a silicon substrate illuminated by an evanescent wave (Loke & Mengüç, 2010), the field intensity indicates where and how much relative heating occurs in the nanostructures. Experiments by Hawes et al. (2008) have shown that it was possible to selectively melt a nanoparticle in a similar configuration.

The scattered near field can be calculated using (18). However, due to the presence the substrate, the contribution from the image dipoles (Fig. 12) will need to be added as per (32). The total field (20) is just the superposition of the incident and scattered fields.

To calculate the internal field, we have to note that (18) cannot be used at the dipole coordinate where a singularity exists. Instead, the E-field of the cubic element in which the point dipole resides can be calculated as follows:

$$\mathbf{E}'_j = \mathbf{E}_{inc,j} - \sum_{k \neq j} \mathbf{A}_{jk} \mathbf{P}'_j, \tag{33}$$

where $\mathbf{P}'_j$ is the dipole moment of the cubic element calculated using the molecular dipole moment formula from section 4.5 of Jackson (1998),

$$\mathbf{P}'_j = \alpha_j \mathbf{E}_j + \frac{1}{3}\mathbf{P}_j. \tag{34}$$

We assume that the cubic element is sufficiently small such that its field approximately uniform.

With the total near and internal field calculations at hand we can plot the field intensity distribution (Fig. 15), demonstrating the effect an AFM probe in the vicinity of a nanoparticle that sits on a planar surface, under evanescent wave illumination. The 3D field distribution plot provides a visual and intuitive feel for the dynamics of such a system.

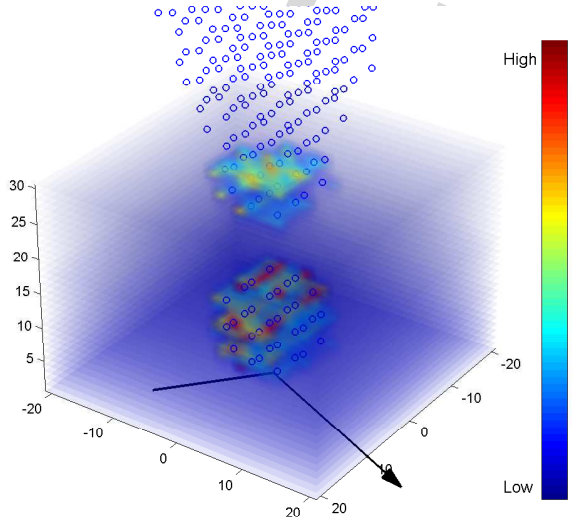

Figure 15: Relative field intensity in the region comprising a simulated gold AFM probe tip in the vicinity of a 20 nm gold nanoparticle on a silicon surface, illuminated by an evanescent wave.

10 Dipole forces

The AFM probe causes a highly localized and intense field in the vicinity of the probe tip and particle; high field gradients exist will result in significant optical forces. Each dipole in the DDA model can be treated as a Rayleigh particle and, on that basis, we propose that the gradient and scattering forces exerted on a dipole can be calculated based on formulae by Harada & Asakura (1996). The gradient force is given by

$$F_{grad} = \frac{2\pi n_1 a^3}{c}\left(\frac{m^2-1}{m^2+2}\right)\nabla I(\mathbf{r}), \tag{35}$$

where n_1 is the refractive index of the surrounding medium, a is taken as the half the lattice spacing, m is the relative refractive index and $\nabla I(\mathbf{r})$ are the intensity gradients in directions of the 3 Cartesian axes, and the scattering force is given by

$$F_{scat} = \hat{z}\frac{n_2}{c}\frac{8}{3}\pi(ka)^4 a^2\left(\frac{m^2-1}{m^2+2}\right)^2 I(\mathbf{r}), \tag{36}$$

where $\hat{z}$ is the unit vector in the direction of propagation of a focussed beam. Figure 16 shows the gradient force vectors resulting from the AFM probe-

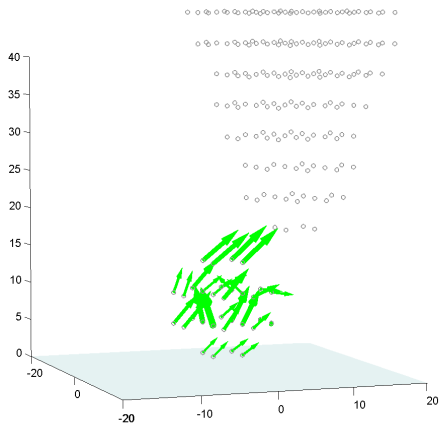

Figure 16: The gradient force vectors of the dipoles in a nanoparticle on a substrate, resulting from a simulated AFM probe placed in its vicinity.

particle-surface coupling. The total force exerted on the particle is just the aggregate of all the force vectors of the dipoles in its lattice. Further investigation will be required to determine the feasibility of the AFM probe 'tractor' moving or aligning nanoparticles on a substrate. The function for calculating the gradient forces for the dipoles is:

```
F = F_grad(E0,kvec,r,d,n_1,n_2,n_3,R_F,P)
```

Acknowledgments

The free-space DDA, symmetry optimization and T-matrix code was developed as part of the PhD. of the first author supervised by the third author at The University of Queensland. The development of the DDA-SI code was funded by a TUBITAK-1001 (Grant No: 109M170) and an FP-7-PEOPLE-IRG-2008 (Grant No: 239382 NF-RAD), carried out at Özyegin University, Istanbul, Turkey.

A List of variables for the MATLAB toolbox

`A`	interaction matrix
`alph`	polarizability particle(s)/scatterer(s)
`d`	lattice spacing
`E0`	Complex amplitude vector of the incident E-field
`E1s`	TE incident E-field amplitude in the substrate
`E1p`	TM incident E-field amplitude in the substrate
`E2s`	TE E-field amplitude in the upper medium
`E2p`	TM E-field amplitude in the upper medium
`Ei`	incident field
`k`	wave number
`k_0`	wave number in air/vacuum
`k_1`	wave number in substrate
`k_2`	wave number in upper medium
`kvec`	wave vector $[k_x\ k_y\ k_z]$
`m`	relative refractive index (scatterer to surrounding medium)
`N`	number of dipoles
`n_1`	refractive index of substrate
`n_2`	refractive index of upper medium
`n_3`	refractive index of particle(s)/scatterer(s)
`P`	dipole moment
`r`	$N \times 3$ dipole coordinates
`r_E`	evaluation point
`R_F`	reflection coefficient
`refl_TE`	Fresnel reflection for the TE mode
`refl_TM`	Fresnel reflection for the TM mode
`gamma`	incident angle

References

A. Baños (1966). *Dipole radiation in the presence of a conducting half-space*. Pergamon Press, Oxford.

E. Bae, et al. (2008). 'Application of the discrete dipole approximation for dipoles embedded in film'. *J. Opt. Soc. Am. A* **25**(7):1728–1736.

P. C. Chaumet & A. Rahmani (2009). 'Efficient iterative solution of the discrete dipole approximation for magnetodielectric scatterers'. *Opt. Lett.* **34**(7):917–919.

W. C. Chew (1990). *Waves and fields in inhomogeneous media*. Van Nostrand Reinhold, New York.

B. Draine (1988). 'The discrete-dipole approximation and its application to interstellar graphite grains'. *Astrophys. J.* **333**:848–872.

B. T. Draine & P. J. Flatau (1994). 'Discrete-Dipole Approximation For Scattering Calculations'. *J. Opt. Soc. Am. A* **11**(4):1491–1499.

B. T. Draine & J. Goodman (1993). 'Beyond Clausius–Mossotti: wave propa-

gation on a polarizable point lattice and the discrete dipole approximation'. *Astrophys. J.* **405**:685–697.

C. E. Dungey & C. F. Bohren (1991). 'Light-scattering By Nonspherical Particles - A Refinement To the Coupled-dipole Method'. *J. Opt. Soc. Am. A* **8**(1):81–87.

G. H. Goedecke & S. G. O'Brien (1988). 'Scattering By Irregular Inhomogeneous Particles Via the Digitized Greens-function Algorithm'. *Appl. Opt.* **27**(12):2431–2438.

J. I. Hage & J. M. Greenberg (1990). 'A Model For the Optical-properties of Porous Grains'. *Astrophys. J.* **361**(1):251–259.

Y. Harada & T. Asakura (1996). 'Radiation forces on a dielectric sphere in the Rayleigh scattering regime'. *Opt. Commun.* **124**:529–541.

E. A. Hawes, et al. (2008). 'Spatially selective melting and evaporation of nanosized gold particles'. *Opt. Lett.* **33**(12):1383–1385.

J. D. Jackson (1998). *Classical electrodynamics*. Wiley, New York. 3rd ed.

F. M. Kahnert, et al. (2003). 'Surface-integral formulation for electromagnetic scattering in spheroidal coordinates'. *JQSRT* **77**(1):61–78.

T. Lemaire (1997). 'Coupled-multipole formulation for the treatment of electromagnetic scattering by a small dielectric particle of arbitrary shape'. *J. Opt. Soc. Am. A* **14**(2):470–474.

V. L. Y. Loke & M. P. Mengüç (2010). 'Surface waves and AFM probe-particle near-field coupling: Discrete dipole approximation with surface interaction'. *J. Opt. Soc. Am. A* **27**(10):2293–2303.

V. L. Y. Loke, et al. (2009). 'T-matrix calculation via discrete-dipole approximation, point matching and exploiting symmetry'. *JQSRT* **110**:1460–1471.

V. L. Y. Loke, et al. (2010). 'Modelling of high numerical aperture imaging of complex scatterers using T-matrix method'. *in Proceedings of ELS XII Helsinki* pp. 138–141.

V. L. Y. Loke, et al. (????). 'User Manual for Discrete Dipole Approximation with Surface Interaction (DDA-SI) for MATLAB'. `http://www.scattport.org/index.php/programs-menu/DDA-SI-menu`.

R. J. Lytle & D. L. Lager (1974). 'Numerical evaluation of Sommerfeld Integrals'. Tech. Rep. UCRL-51688, Lawrence Livermore Laboratory, Livermore, California.

D. W. Mackowski (2002). 'Discrete dipole moment method for calculation of the T-matrix for nonspherical particles'. *J. Opt. Soc. Am. A* **19**(5):881–893.

M. I. Mischenko, et al. (2000). *Light scattering by nonspherical particles: theory, measurements and applications*. Academic Press, San Diego.

M. I. Mishchenko (1991). 'Light scattering by randomly oriented axially symmetrical particles'. *J. Opt. Soc. Am. A* **8**(6):871–882.

G. W. Mulholland, et al. (1994). 'Light-scattering By Agglomerates - Coupled Electric and Magnetic Dipole Method'. *Langmuir* **10**(8):2533–2546.

B. M. Nebeker (1998). *Modeling of light scattering from features above and below surfaces using the discrete-dipole approximation*. Ph.D. thesis, Arizona State University. AAT 9837688.

T. A. Nieminen, et al. (2003a). 'Calculation of the T-matrix: general considerations and application of the point-matching method'. *JQSRT* **79-80**:1019–1029.

T. A. Nieminen, et al. (2003b). 'Multipole expansion of strongly focussed laser beams'. *JQSRT* **79-80**:1005–1017.

T. A. Nieminen, et al. (2007). 'Optical tweezers computational toolbox'. *J. Opt. A* **9**:S196–S203.

E. Purcell & C. Pennypacker (1973). 'Scattering and Absorption of Light by Nonspherical Dielectric Grains'. *Astrophys. J.* **186**:705–714.

R. Schmehl, et al. (1997). 'Discrete-dipole approximation for scattering by features on surfaces by means of a two-dimensional fast Fourier transform technique'. *J. Opt. Soc. Am. A* **14**(11):3026–3036.

A. Sommerfeld (1909). 'Über die Ausbreitung der Wellen in der drahtlosen Telegraphie'. *Ann. Physik* **28**:665–736.

M. A. Taubenblatt & T. K. Tran (1993). 'Calculation of light scattering from particles and structures on a surface by the coupled-dipole method'. *J. Opt. Soc. Am. A* **10**(5):912–919.

H. C. van de Hulst (1957). *Light scattering by small particles*. Wiley, New York & London.

P. C. Waterman (1971). 'Symmetry, Unitarity, And Geometry In Electromagnetic Scattering'. *Phys. Rev. D* **3**(4):825–839.

T. Wriedt (2009). 'Light scattering theories and computer codes'. *JQSRT* **110**(11):833–843.

T. Wriedt & U. Comberg (1998). 'Comparison of computational scattering methods'. *JQSRT* **60**(3):411–423.

M. Yurkin, et al. (2007). 'The discrete dipole approximation for simulation of light scattering by particles much larger than the wavelength'. *JQSRT* **106**:546–557.

M. A. Yurkin & A. G. Hoekstra (2007). 'The discrete dipole approximation: An overview and recent developments'. *JQSRT* **106**(1-3):558–589.

H. Zhang & E. D. Hirleman (2002). 'Prediction of light scattering from particles on a filmed surface using discrete-dipole approximation'. *Proceedings of SPIE* **4692**:38–45.